JOURNAL OF BIOMEDICAL OPTICS 4(3), 376–380 (JULY 1999)

# LYMPHOCYTE NUCLEUS RECONSTRUCTION VIA WAVELET TOMOGRAPHY

**Igor Patrickeyev and Peter Frick**
**Institute of Continuous Media Mechanics, Korolyov 1, Perm, 614061, Russia**

(Paper JBO-210 received Aug. 1, 1998; revised manuscript received Apr. 20, 1999; accepted for publication May 4, 1999. )

## ABSTRACT

A wavelet tomographic algorithm is presented for statistical reconstruction of a lymphocyte nucleus. The investigation is concerned with lymphocyte nuclei of peripheral blood from two groups of patients: those who live in the area affected by the Chernobyl accident and the control group. The purpose of reconstruction is to find the probability density function of radial distribution of condensed chromatin. The difference between the two test groups is seen from considering the results of reconstruction and the wavelet energy spectra. The Radon transform is treated here as a singular wavelet transform, which allows us to reconstruct the essential scales from projection and to denoise them simultaneously. The algorithm of reconstruction involves back projecting and continuous wavelet synthesis with denoising. The use of a special local filter insures the stability of reconstruction. © *1999 Society of Photo-Optical Instrumentation Engineers.* [S1083-3668(99)00603-6]

**Keywords** lymphocyte; chromatin; tomography; singular wavelets; continuous wavelet transform; energy decomposition.

## 1 INTRODUCTION

The three-dimensional (3D) analysis of a nucleus is required to study the mechanism of interphase structural regulation and has wide application in early diagnostics of diseases. The problem of *tomographic reconstruction* arises from the necessity to analyze the *spatial* structure of a nucleus by optical microscopy. All known methods are based on examination of the two-dimensional (2D) projection and can be used to study plane structures only.[1,2] The algorithm proposed is an attempt to reconstruct the 3D structure from 2D projection.

The initial assumption for reconstructing the nucleus is that intranuclear chromatin is radially arranged on the supramolecular level. ''Cytologically, chromatin is classified into condensed and diffuse... . This classification holds for most cell nuclei. The condensed (DNA-containing) structures make up 15% to 30% of total area, occupied by nuclear material. The two types of chromatin also differ functionally.'' [1] Under the light microscope the interphase nucleus looks like a halftone image of dark (granular) and light (nongranular) areas. The granular areas correspond to condensed chromatin and demonstrate the low genetic activity. The nongranular areas correspond to diffused chromatin and indicate strong genetic activity.[1] The hypothesis for the radial symmetry of distribution of granules is frequently used as a first approximation and will be employed in our investigation. Thus, the statistical reconstruction of condensed chromatin 3D structure in a spherical coordinate system is reduced to restoration of the radial distribution.

The second assumption implies that the image acquired from the optical microscope can be considered as the projection of a nucleus onto the plane at random angle. A set of representative images makes it possible to reconstruct the radial symmetric probability density function (PDF) or, at least, its large-scale structure. Theoretically, the reconstruction of the unique nucleus structure is feasible but in practice the noise, distorting the data, decreases the accuracy of reconstruction. Therefore, we restrict our task to reconstruction of the averaged large-scale density distribution. In the context of this problem it is favorable to use an algorithm, which includes the scale separation in a generic way. Wavelets seem to be suitable for this objective. We have used the results by Holschneider, which demonstrate how to use the inverse wavelet transform for computing the inverse Radon transform in the 2D case.[3,4] With these ideas we have developed a program which inverts the discrete Radon data only for the radial symmetric function and is adapted to noisy data. The program has been tested for several benchmark signals with various levels of noise. For stable reconstruction, a local filter was designed and applied.

In this work, use is made of the arrays of normalized radius vectors of granule centers of lymphocytes of peripheral human blood obtained by the morphodensitometry method.[1] Individuals were divided into two groups: those who live in the area

Further author information, contact Igor Patrickeyev, e-mail: pat@icmm.ru; http://plaxa.icmm.ru/~lab4/igor.htm; Tel: 7 3422 391258; Fax: 7 3422 336957, or Peter Frick, e-mail: frick@icmm.ru; http://plaxa.icmm.ru/~lab4/frick.htm; Tel: 7 3422 391258; Fax: 7 3422 336957.

affected by the Chernobyl accident (Group I) and others who live outside this area, i.e., control Group II. All morphodensitometric data were kindly granted by A. Zhukotsky.

On the hypothesis that chromatin is radially symmetric arranged, we have taken the proposed method for nucleus reconstruction. The main question was how to distinguish between two groups on the supramolecular level. For each group we constructed its own histogram indicating the distribution of radius vectors over the rings of equal area in the projection of a nucleus. Considering these histograms as the Radon data, we have reconstructed the central profile of a nucleus for Groups I and II. Finally, we have compared the wavelet energy spectra for these groups.

## 2 SINGULAR WAVELET TRANSFORM AND ABEL EQUATION

For the sake of completeness we briefly review the main notions of the 2D continuous wavelet transform. The set of wavelets over the plane $\mathbf{R}^2$ is generated with respect to the function $g$ by applying the 2D translation $T$, dilation $D$, and, in the case of anisotropic wavelet, rotation $\Omega$,[3,4]

$$(T^{b_x,b_y}g)\begin{bmatrix}x\\y\end{bmatrix}=g\begin{bmatrix}x-b_x\\y-b_y\end{bmatrix},$$

$$(D^a g)\begin{bmatrix}x\\y\end{bmatrix}=a^{-2}g\begin{bmatrix}a^{-1}x\\a^{-1}y\end{bmatrix}, \tag{1}$$

$$(\Omega^\varphi g)\begin{bmatrix}x\\y\end{bmatrix}=g\left(\begin{bmatrix}\cos\varphi & -\sin\varphi\\ \sin\varphi & \cos\varphi\end{bmatrix}\begin{bmatrix}x\\y\end{bmatrix}\right).$$

The continuous wavelet transform with parameters $b_x$, $b_y$, $a$, $\varphi$ is defined as a convolution of the function $f$ with the wavelet $g$:

$$Wf(b_x,b_y,a,\varphi)=\int_{\mathbf{R}^2}\int f(x,y)(T^{b_x,b_y}D^a\Omega^\varphi g)\times(x,y)dx\,dy. \tag{2}$$

Thus, the 2D wavelet transform maps the function $f(x,y)$ onto the four-dimensional space. For a more precise description of the 2D continuous wavelet transform, we refer to Ref. 3.

For the radially symmetric function $f(p)$, the translation $T$ depends on the radial coordinate only, and the wavelet space is reduced to the three-dimensional case

$$Wf(b,a,\varphi)=\int_{\mathbf{R}^2}\int f(p)(T^bD^a\Omega^\varphi g)(x,y)dx\,dy, \tag{3}$$

where

$$p=\sqrt{x^2+y^2},\quad b=\sqrt{b_x^2+b_y^2}. \tag{4}$$

The projection data acquisition is traditionally simulated using the Radon transform. In the 2D case, the Radon transform is defined as the set of integrals along all straight lines $s$ with parameters $p$ and $\varphi$,[3–5]

$$Rf(p,\varphi)=\int_{-\infty}^{\infty}f(p\cos\varphi-s\sin\varphi,p\sin\varphi+s\cos\varphi)ds. \tag{5}$$

In view of the fact that the integral of $f$ along the straight line is equal to the integral over the whole plane of the product $f$ and the $\delta$ function concentrated on this straight line, the previous equation is written as

$$Rf(p,\varphi)=\int_{\mathbf{R}^2}\int f(x,y)\delta(x\cos\varphi+y\sin\varphi-p)dx\,dy, \tag{6}$$

where the argument of the $\delta$ function is taken from the left-hand part of the secant line equation

$$x\cos\varphi+y\sin\varphi-p=0. \tag{7}$$

Since every straight line can be obtained from the line $x=0$ by translation and rotation, then the Radon transform can be defined in terms of the wavelet transform[3,4] as

$$Rf(p,\varphi)=\int_{\mathbf{R}^2}\int f(x,y)(T^p\Omega^\varphi\delta)(x)dx\,dy. \tag{8}$$

Consequently, the Radon transform can be considered as a wavelet transform with singularity. The singular $\delta$ function differs from the regular wavelets and its mean value is not equal to zero. Moreover, the regular wavelets are localized simultaneously in signal and frequency spaces. Singular wavelets are concentrated in the infinitesimal domain and, therefore, have infinite spectrum, or, in other words, the $\delta$ function does not obey the admissibility condition.[3]

The $\delta$ function as a singular wavelet has some specific features, such as the invariance to dilation, allowing us to establish the link between the singular wavelet transform of function $f$ and its Radon transform[3,4]

$$Wf(b_x,b_y,a,\varphi)=\frac{1}{a}Rf(p',\varphi), \tag{9}$$

where $p'$ is governed by the formula known in tomography as ''back projection''[5]

$$p'=b_x\cos\varphi+b_y\sin\varphi. \tag{10}$$

For the radially symmetric function, Eq. (6) is reduced to the Abel equation, because the function and its Radon image are independent of $\varphi$

$$Af(p)=2\int_p^\infty\frac{rf(p)}{\sqrt{r^2-p^2}}dr. \tag{11}$$

The Abel equation (11) is considered as a particular case of the Radon transform and can be redefined through the singular wavelet transform using Eq. (8),

$$Af(p)=\int_{\mathbf{R}^2}\int f(x,y)(T^p\delta)(x)dx\,dy. \qquad (12)$$

Substituting (10) with $b_x=b$, $b_y=0$ into (11) gives

$$Wf(b,a,\varphi)=\frac{1}{a}Af(b\cos\varphi). \qquad (13)$$

It should be noted that the behavior of singular wavelet image (11) or (13) is the same at any scale $a$.

Equations (11) and (13) make it possible to apply the wavelet potentialities (singularity detection, energy spectrum analysis, etc.) in reconstructing the function from its projection.

## 3 STABLE TOMOGRAPHIC RECONSTRUCTION VIA WAVELET SYNTHESIS

The reconstruction of the function from its singular wavelet image is realized by convolution with a synthesizing wavelet and by integration with respect to the angle coordinate $\varphi$ and the scale coordinate $a$. For the Radon transform, the choice of synthesizing wavelet $h$ is made under the following restriction:[3,4]

$$\int_{-\infty}^{\infty}\frac{d\gamma}{|\gamma|^2}\hat{h}(\gamma\vec{e})=2\pi, \qquad (14)$$

where $\vec{e}=(\cos\varphi,\sin\varphi)$, $\hat{h}$ is the Fourier image of synthesizing wavelet, and $\gamma$ is the radial frequency

$$\hat{h}(\gamma)=\int_{-\infty}^{\infty}h(p)e^{-i\gamma p}\,dp. \qquad (15)$$

Expression (14) allows us to compensate the singularity of the analyzing wavelet by choosing the suitable regular wavelet at the stage of synthesis.

For the radial symmetrical function synthesized at a single scale, $a$ is defined by a convolution of the singular wavelet image $Wf$ with $h(p)$ taken under condition (14). From (13) it follows that

$$\tilde{f}(p,a)=a^{-2}\int_0^{2\pi}d\varphi\int_{-\infty}^{\infty}Af(b)h\left(\frac{b-p\cos\varphi}{a}\right)db. \qquad (16)$$

For complete reconstruction of the function from its wavelet image, the following inversion holds:[3,4]

$$f(p)=\lim_{\epsilon\to 0,\rho\to\infty}\frac{1}{C^2}\int_{\epsilon}^{\rho}\tilde{f}(p,a)\frac{da}{a}, \qquad (17)$$

where $C$ is the normalizing coefficient.

The appropriate synthesizing wavelet is chosen under such conditions as resolving power of wavelet, etc. For example, the Mexican hat function meets condition (14) and can be used to reconstruct the function from its projection

$$h(p)=(1-p^2)\exp(-p^2/2). \qquad (18)$$

For the Mexican hat function, $C=2\pi$. This wavelet has been used in our work.

The exact reconstruction of the function from its projection described above is unstable in the event we use the noisy projection data. Let the projection data be distorted by the additive noise $\eta$; then

$$f(p)=\lim_{\epsilon\to 0,\rho\to\infty}\frac{1}{C^2}\int_{\epsilon}^{\rho}\frac{da}{a}\int_0^{2\pi}d\varphi\int_{-\infty}^{\infty}(Af+\eta)\times a^{-2}h\left(\frac{b-p\cos\varphi}{a}\right)db. \qquad (19)$$

The internal integral can be considered as a convolution with a high-pass filter. From (19) it is seen that there will be amplification of the small-scale components of noisy projection data. If the level of noise on small scales is high, then the regularizing filter is required for stable reconstruction.[5] The elementary variant of regularization is to restrict small scales during integration. In this case no fine details (at $a<a_{\min}$) are restored at any point of $p$. This way of regularization is similar to the low-pass filtering in classical tomography.[5] The local filtering of the function at each point depending on its behavior is a more complicated procedure. One such filter will be described in the next section.

## 4 RECONSTRUCTION OF LYMPHOCYTE NUCLEUS

Consider the granule center radius vectors in a lymphocyte nucleus. The geometry of projections is shown in Figure 1. Each nucleus usually contains 10–15 granules of condensed chromatin. Unfortunately, the small number of granules does not allow the reconstruction of the nucleus structure from unique projection. However, the superposition of many nuclei gives enough data for the reconstruction of averaged (statistical) values. In this article, lymphocytes of peripheral human blood from the area affected by the Chernobyl accident (Group I) and from the control Group II are studied. The total number of granules comprises 820 and 819 for Groups I and II, respectively.

Histograms of radius vectors are constructed for each group. For this, the nucleus projection is divided into 16 rings and the number of radius vectors on each ring is counted. Histograms for each group are shown in Figure 2. In this case, the projecting can be mathematically treated as a random hit onto the plane; therefore the nucleus projection

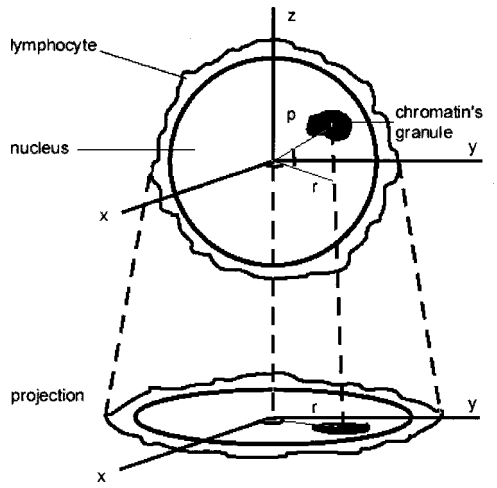


**Fig. 1** Geometry of projections. Three-dimensional lymphocyte is projected to the plane during specimen preparation; *p*—distance from the center of nucleus (3D radial coordinate) to the center of granule, *r*—distance from the center of nucleus projection (2D radial coordinate) to the center of granule projection. Total number of granules is 1639 (belong to more than 100 lymphocyte nuclei).

is divided into rings of *equal area*. Hence, the ring width decreases from the nucleus center to its circumference.

We consider these histograms as the projection data. The reconstruction of statistical distribution of granules in a lymphocyte nucleus was made using

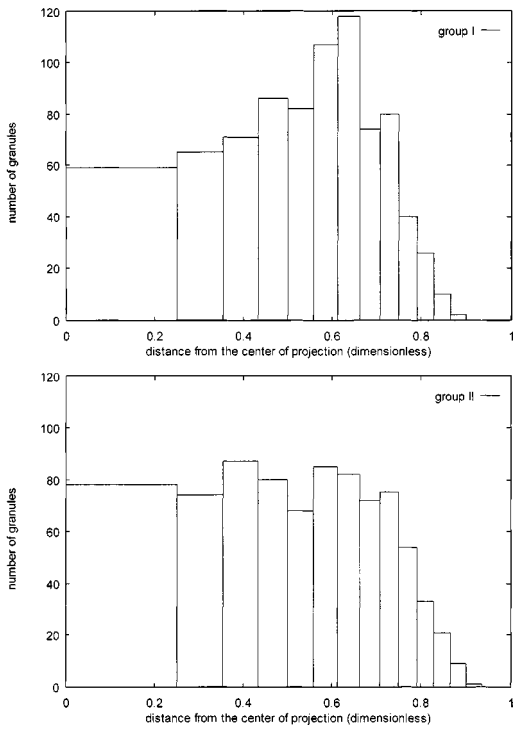


**Fig. 2** Histograms of radius vectors of the centers of granule's projections. All radius vectors are normalized to the radius of the nucleus projection. Number of granules is counted among the rings of equal area. *Top*: Affected territories (Group I); *bottom*: control group (Group II).

the Mexican hat function (18) as a synthesizing wavelet for each group. The parameters taken were as follows: the number of reconstructed points is 64, and the scale $a$ ranges from $a_{\min}=0.02$ to $a_{\max}=4$.

A more stable reconstruction with these parameters can be achieved if the values of the wavelet image at small $a$ corresponding to high frequencies are reduced to the nucleus circumference. This encourages us to carry out further reconstruction with a special (designed *ad hoc*) local filter

$$q(p,a)=\exp\left(-\frac{p^2}{2\sigma^2(a)}\right), \tag{20}$$

where $\sigma$ is proportional to the scale $a$ and is written as

$$\sigma(a)=\frac{\sigma_{\max}-\sigma_{\min}}{a_{\max}-a_{\min}}(a-a_{\min})+\sigma_{\min}. \tag{21}$$

In this case, for experimental data processing the following formula is used, which provides a stable but approximate reconstruction:

$$f(p)=\lim_{\epsilon\to 0,\rho\to\infty}\frac{1}{C^2}\int_{\epsilon}^{\rho}\frac{da}{a}\int_0^{2\pi}d\varphi\left[q(p,a)\int_{-\infty}^{\infty}(Af+\eta)\times a^{-2}h\left(\frac{b-p\cos\varphi}{a}\right)db\right], \tag{22}$$

where $Af+\eta$ changes to the histogram interpolated through the ring centers for both groups.

Figure 3 presents the reconstruction results of the statistical distribution of granule centers (a) without a filter, (b) with a classical Ramachandran–Lakshminarayanan (Ram–Lak) filter,[5] and (c) with a wavelet-based filter (20) at $\sigma_{\min}=0.5$, $\sigma_{\max}=50$. An *a priori* condition, PDF$>0$, is provided by imposing the additional restriction on the small-scale noise near the nucleus center.

As seen from Figure 3, the groups have different PDFs. A statistical distribution of granules (condensed chromatin) in a lymphocyte nucleus from Group I is close to the Gaussian function with a maximum near $p_0=0.7$. The maximum is well defined on the plot both with regularization and without it. The PDF in the central region ($|p|<0.5$) is about zero; that is, no granules exist in the vicinity of the nucleus center. The granule distribution in lymphocyte nuclei from Group II is more uniform as compared to Group I; however, some maximums and minimums are observed. In the vicinity of the nucleus center the PDF is nonzero. The nonregularized and globally regularized filters amplify the small-scale components of noisy projection data, which explains the artifact that PDF is negative in some intervals.

The difference between Groups I and II is readily seen from their wavelet energy spectra, sometimes called the ''energy-scale decompositions,'' which are governed by

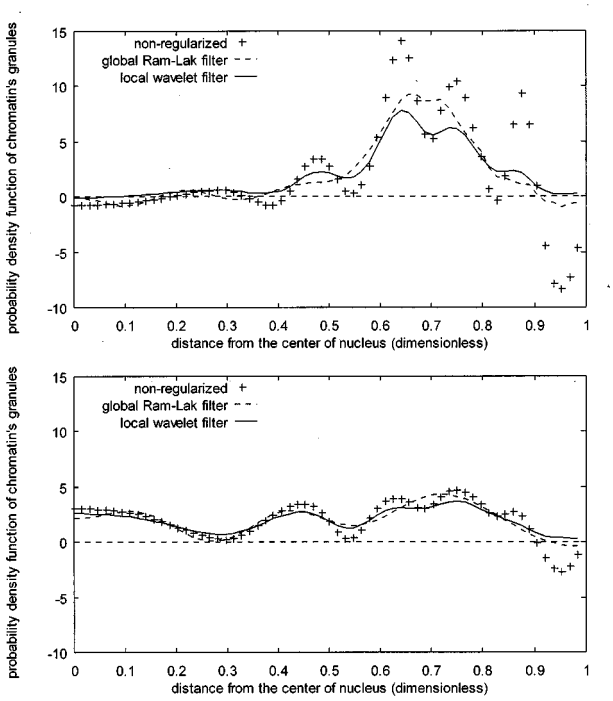


**Fig. 3** Reconstructed 3D probability density function under radially symmetric approximation. Each plot consists of three curves: (a) without a filter, i.e., through the nonregularized algorithm (*crosses*), (b) with a classical tomographic Ram–Lak filter that passes the ten lowest frequences and provides the global regularization (*dashed line*), and (c) with a wavelet-based filter that provides denoising depending on the radial coordinate (*solid line*). *Top*: Affected territories (group I); *bottom*: control group (Group II).

$$Ef(a) = \int_{-\infty}^{\infty} |\tilde{f}(b,a)|^2 \, db. \tag{23}$$

The wavelet energy spectra for Groups I and II are shown in Figure 4. Abscissa is the scaling parameter $a$ in the log scale.

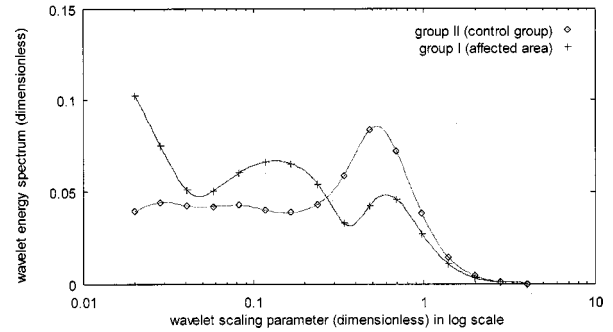


**Fig. 4** Wavelet energy spectra of both groups. Each spectrum is calculated at 16 values of scaling parameter $a$ and then smoothed with cubic spline. Total energy is normalized to 1.

Figure 4 shows that the wavelet energy spectra of Groups I and II have their maxima in different parts of the scale. For Group II one maximum is observed. This means that the most energy is localized on the large scales. Vice versa, for Group I the main energy maximum shears to the medium scales, and the local maximum exists on the large scales. The bend of the curves on the smallest scale is probably explained by noise.

## 5 CONCLUSION

We have applied the wavelet tomography algorithm to study the chromatin density distribution in a lymphocyte nucleus. Wavelets enable us to denoise the projection data and to reconstruct the large-scale structures simultaneously. The statistical reconstruction of a lymphocyte nucleus has been done for two groups of patients: those who live in the area affected by the Chernobyl accident, and the control group. We have obtained the 3D probability density function (PDF) of condensed chromatin in a radially symmetric approximation using histograms of granule distribution in 2D projection. In addition, the energy-scale decomposition has been done for both groups. To make the stable reconstruction of the PDF, a specific regularizing filter was designed and used. It has been found that the groups have different PDFs and energy-scale decompositions. According to the PDF, there are no granules in the nucleus center for Group I. The granule distribution in a lymphocyte nucleus for Group II is more uniform as compared to Group I. Based on the energy-scale decomposition, we can conclude that the large-scale structures of granules dominate for Group I, and for Group II there are the additional middle-scale structures.

### Acknowledgment

We thank A. V. Zhukotsky, Moscow Institute for Physical and Chemical Medicine, for granted morphodensitometric data.

## REFERENCES

1. A. V. Zhukotsky and E. M. Kogan, ''Automated analysis of chromatin structure in interphase cell nuclei,'' *Sov. Med. Rev. Physicochem. Asp. Med.* **2**, 25–77 (1989).
2. P. Bartels, ''Computer analyses of lymphocyte image,'' *Methods of Cell Separation*, N. Castssimpoolas, Ed., Vol. 3, pp. 1–100, Plenum, New York (1980).
3. M. Holschneider, *Wavelets: An Analysis Tool*, p. 423, Oxford Univ. Press, London (1995).
4. M. Holschneider, ''Inverse Radon transform through inverse wavelet transform,'' Prep. No. P2364 CPT90, C.N.R.S. (Feb. 1990).
5. F. Natterer, *The Mathematics of Computerized Tomography*, Wiley, New York (1986).